Complex energy approaches for calculating isobaric analogue states

R. Id Betan
Departamento de Química y Física, FCEIA(UNR)-Instituto de Física Rosario (CONICET), Avenida Pellegrini 250, 2000 Rosario, Argentina

A. T. Kruppa
Institute of Nuclear Research of the Hungarian Academy of Sciences, Post Office Box 51, H-4001 Debrecen, Hungary

T. Vertse
Institute of Nuclear Research of the Hungarian Academy of Sciences, Post Office Box 51, H-4001 Debrecen, Hungary and University of Debrecen, Faculty of Informatics, Post Office Box 12, H-4010 Debrecen, Hungary
(Received 30 June 2008; published 14 October 2008)

Parameters of isobaric analog resonance (IAR) are calculated in the framework of the Lane model using different methods. In the standard method, the direct numerical solution of the coupled channel (CC) Lane equations served as a reference for checking two complex energy methods, namely the complex energy shell model (CXSM) and the complex scaling (CS) approaches. The IAR parameters calculated by the CXSM and the CS methods agree with that of the CC results within 1 keV for all partial waves considered. Although the CXSM and the CS methods have similarities, an important difference is that only the CXSM method offers a direct way for studying the configurations of the IAR wave function.

DOI: 10.1103/PhysRevC.78.044308 PACS number(s): 21.10.Sf, 24.30.Gd, 24.10.Eq, 21.60.Cs

I. INTRODUCTION

The isobaric analog resonance (IAR), discovered about four decades ago, appears because of the approximate isospin symmetry of the states in isobaric nuclei. The parent and the analog states would be degenerate if the isospin were a good quantum number, but Coulomb forces break the degeneracy and shift the analog states up from the parent state. Therefore in medium and heavy nuclei where the Coulomb energy shift is large enough the analog state becomes a resonance.

Recently, IAR has attracted interest again during the study of the light exotic nuclei being in the drip line region. Here a smaller value of the Coulomb energy difference can produce IAR because the parent state is weakly bound. The unusual properties of neutron-rich nuclei provide insights into the nuclear structure far from the valley of stability. The extreme neutron to proton ratios might help in understanding the nuclear matter at extreme conditions. However, the experimental study of the neutron-rich nuclei around the neutron drip line is difficult. Since the IAR has essentially the same structure as the parent state it was suggested that instead of the neutron-rich exotic nuclei (e.g., ^{11}Li, ^{14}Be, ^{7}He, and ^{9}He) [1–4] their less exotic analog states should be studied (with inverse kinematics) to gain information on the properties of these exotic nuclei.

New developments in experimental facilities opened the possibility of identifying a large number of exotic nuclei. To understand the structure of these nuclei new theoretical methods have been developed for describing the dynamics of weakly bound or unbound nuclei from which nucleons can be emitted. Some of the new methods—for example, the shell model in the complex energy plane (CXSM) [5,6] or the Gamow shell model [7–11]—use the Berggren basis [12]. In the Berggren basis bound and resonant states are treated on equal footing and scattering states taken along a contour L of the complex energy sheet are included. This will be discussed later in detail. In the past few years this basis has been used successfully in a series of works [13–17]. Since the extended use of this basis started not very long ago we think that it is worthwhile to accumulate more experience concerning its use, namely the accuracy and the parameter dependence of the methods in which this basis is used.

Another well-established method for calculating resonances is the complex scaling (CS) method. Complex scaling has a strict mathematical foundation given in Refs. [18–20]. The possible applications and the details of the CS method are reviewed in Refs. [21,22].

The IAR phenomenologically can be described by the Lane equations [23] or can be studied microscopically [24]. Coupled channel (CC) Lane equations offer a simple but not trivial example (the simplest multichannel example) in which both the CXSM and the CS approaches can be checked.

Our aim in this work is to compare the parameters of the IAR calculated by different methods. We shall compare the characteristic features of the two methods working on the complex energy plane. The experiences of a methodical work like this might be useful later in analyzing experimental data in more realistic calculations.

The CS approach can be applied only for dilation analytic potentials and interactions. Some of the widely used nuclear potentials are either not dilation analytic or are dilation analytic only in a limited range of the rotation angle (i.e., below the critical value of the rotation angle). Therefore we repeat our calculation with a slightly modified Coulomb potential that is dilation analytic. This comparison is very useful for comparing the accuracy of the CXSM and CS methods in cases when both methods can be applied.

In Sec. II A we summarize the features of the Lane equations. In Sec. II B we describe the approximate solution

of the Lane equations using the CXSM, and in Sec. II C we present a short description of the solution of the Lane equations using CS. In Sec. III we give the numerical results of the calculations. In the first part of Sec. III we compare the positions of the poles of the S matrix calculated by the CXSM method with those extracted from the solution of the Lane equations. The results of the CS method are also presented here. The similarities and differences of the CXSM and CS methods are also discussed in that section. Finally, in Sec. IV we summarize the main conclusions of the paper.

II. RESONANCE SOLUTION OF THE LANE EQUATIONS

The Lane equations in the simplest case describe the quasielastic scattering of a proton and the IAR. We assume that the target nucleus has mass number $A = N + Z$ and charge number Z. The ground state of the target has isospin T_A and isospin projection $T_3 = \frac{N-Z}{2} = T_A$. The target is bombarded by a beam of protons.

A. Lane equations

The Hamiltonian of the target plus nucleon system, H, can be divided into a part describing the internal motion of the target, $H(\xi)$, and one describing the relative motion, $H_{\rm rel}$, of the nucleon with respect to the target:

$$H = H(\xi) + H_{\rm rel}. \tag{1}$$

The internal state of the ground state of the target is denoted by $|A\rangle$ and this state is the solution of the equation $H(\xi)|A\rangle = \epsilon_A|A\rangle$. The analog nucleus, denoted by $\tilde{A}$, has the same isospin T_A and isospin projection $T_A - 1$. It is an excited state of the isobaric nucleus with $Z + 1$ protons and $N - 1$ neutrons. If we neglect the mass difference between the neutron and proton and denote the additional Coulomb energy of the analog nucleus by Δ_c then the eigenvalue of the internal motion of the analog state is simply $\epsilon_A + \Delta_c$ and we have $H(\xi)|\tilde{A}\rangle = (\epsilon_A + \Delta_c)|\tilde{A}\rangle$. Let $|pA\rangle$ and $|n\tilde{A}\rangle$ be the states formed by adding a proton and neutron to $|A\rangle$ and $|\tilde{A}\rangle$, respectively. The total wave function of the system may be written in the form

$$\Psi = |A\rangle\phi_p(\mathbf{r}) + |\tilde{A}\rangle\phi_n(\mathbf{r}), \tag{2}$$

where $\phi_p(\mathbf{r})$ and $\phi_n(\mathbf{r})$ describe the relative motion. The relative motion part of the total Hamiltonian can be cast into the form

$$H_{\rm rel} = K + V_0(\mathbf{r}) + \hat{\mathbf{t}}\cdot\hat{\mathbf{T}}V_1(\mathbf{r}) + \left(\tfrac{1}{2} - t_3\right)V_C(r), \tag{3}$$

where K is the kinetic energy operator of the relative motion, V_0 comes from the interactions independent from the isospin, V_C is the nuclear Coulomb potential, and $\hat{\mathbf{t}}\cdot\hat{\mathbf{T}}V_1(\mathbf{r})$ is the symmetry term accounting for the isospin-dependent strong interactions. The vector operators $\hat{\mathbf{t}}$ and $\hat{\mathbf{T}}$ are the isospin operators of the nucleon and of the target. Substituting the ansatz [Eq. (2)] into the Schrödinger equation $H\Psi = \mathcal{E}\Psi$ and taking into account the form of the relative Hamiltonian [Eq. (3)] we get the Lane equations [23]:

$$\begin{aligned}
&\left[K + V_0 - \frac{V_1}{2}T_A + V_C - \mathcal{E}_p\right]\phi_p + \sqrt{\frac{1}{2}T_A}V_1\phi_n = 0,\\
&\left[K + V_0 + \frac{V_1}{2}(T_A - 1) - (\mathcal{E}_p - \Delta_c)\right]\phi_n + \sqrt{\frac{1}{2}T_A}V_1\phi_p = 0,
\end{aligned} \tag{4}$$

where $\mathcal{E}_p = \mathcal{E} - \epsilon_A$ is the center-of-mass energy of the relative motion in the proton plus target system and the energy in the neutron plus analog nucleus channel, namely $\mathcal{E}_p - \Delta_c$. If we assume spherically symmetric interactions then the relative motion can be separated into partial waves and no coupling will occur between different partial waves characterized by orbital l and total angular momentum j quantum numbers. We consider this simple case. In the standard method described for example in Ref. [25], we solve the Lane equations by using numerical integration. The numerical solution of the Lane equations is carried out by using a fourth-order Runge-Kutta method. At each real $\mathcal{E}_p$ value we calculate two linearly independent solutions of the coupled equations. The physical solution with components ϕ_p and ϕ_n being regular at $r = 0$ was combined from these independent solutions. These components ϕ_p and ϕ_n were matched to the scattering (or outgoing wave) solutions of the corresponding channels at a distance where the nuclear potentials are cut to zero.

B. CXSM solution using the Berggren basis

In this section we calculate the complex energy eigenvalues of the IAR by diagonalizing the Hamiltonian [Eq. (1)] in the combined Berggren bases [12] of the target plus proton and analog plus neutron systems. First we describe the Berggren basis for the protons. We consider an auxiliary problem, a radial Schrödinger equation with the diagonal potential of the first Lane equation [Eq. (4)],

$$\left[K_l + V_0 - \tfrac{1}{2}T_A V_1 + V_C - E_n^{(p)}\right]u_n^{(p)}(r) = 0, \tag{5}$$

where

$$K_l = -\frac{\hbar^2}{2\mu}\left[\frac{d^2}{dr^2} - \frac{l(l+1)}{r^2}\right]. \tag{6}$$

The discrete bound and resonance solutions with energy $E_n^{(p)}$ are denoted by $u_n^{(p)}(r)$ and the scattering solutions by $u^{(p)}(r, E)$. Sometimes when it is obvious we will use the wave number k instead of the energy E and the scattering states along the contour in the lower half of the second energy sheet will be denoted by $u^{(p)}(r, k)$.

The main advantage of the Berggren basis is that the single-particle basis set consists not only of bound states but also of poles of the single-particle Green function on the complex energy (wave number) planes and a continuum of scattering states taken along a complex contour L. A typical contour of the complex wave number plane is shown in Fig. 1. The L^+ part of the contour goes from the origin to infinity in the lower half of the second energy sheet, whereas the L^- part of

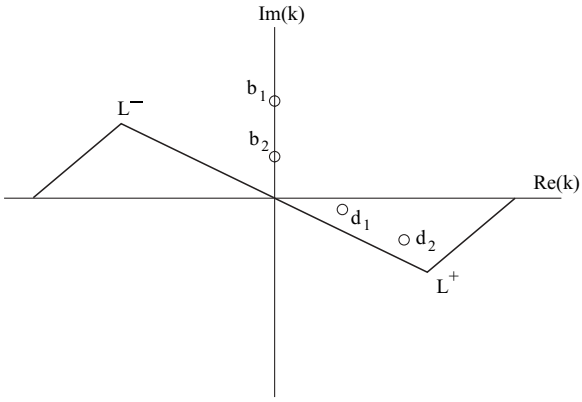

FIG. 1. Positions of the bound (b_1, b_2) and decaying resonant (d_1, d_2) poles of $S(k)$ on the complex k-plane and a possible choice of the complex contour L.

the contour makes exactly the same tour on the first energy sheet. It was observed in Refs. [26,27] that the contour L^+ need not return to the real axis at infinity. The shape of the chosen complex contour $L = L^+ + L^-$ regulates which of the poles should be included in the Berggren basis forming the completeness relation of Berggren:

$$\delta(r - r') = \sum_{n=b,d} u_n^{(p)}(r) u_n^{(p)}(r') + \int_{L^+} dk u^{(p)}(r,k) u^{(p)}(r',k). \tag{7}$$

In this relation (and later) the notation $n = b, d$ means that the sum over n runs through all bound states plus the decaying resonances lying between the real energy axis and the integration contour L^+ of Fig. 1. The integral in Eq. (7) is over the scattering states along L^+. The poles denoted by d in the basis generally correspond to decaying resonances lying on the fourth quadrant of the complex k-plane.

The completeness relation in Eq. (7) was introduced for chargeless particles in Ref. [12] and it has been shown later in Refs. [28,29] that it is valid even for charged particles. Berggren completeness can be generalized by using a contour of different shape in which antibound states [30] lying on the negative part of the imaginary k-axis are included in the sum in Eq. (7). Since the inclusion of antibound states is not optimal as far as the number of basis states is concerned [31] we are not using antibound basis states in this work.

Berggren introduced a generalized scalar product between functions defining a special complex metric of the Berggren space [12]. In the generalized scalar product in the left (bra) position of the scalar product the mirror partner state (denoted by a tilde over the state) is used. This state corresponds to a reflection to the imaginary k-axis. Because of this reflection in this scalar product in the integral the radial wave function itself appears and not the complex conjugate of the radial function. (This causes no difference for bound states lying on the positive part of the imaginary axis.) This is the only modification in the scalar product since the spin-angular degrees of freedom remains unchanged. If the radial integral to be calculated has no definite value then a regularization procedure has to be applied. Zel'dovich [32] and also Romo [33] suggested regularization methods but we use the complex rotation of the radial distance r beyond the range of nuclear forces [34].

The upper half of the complex k-plane maps to the physical (or first) Riemann sheet of the complex energy $E \sim k^2$. The pole wave functions of this sheet are square-integrable functions belonging to bound states. The lower half of the complex k-plane maps to the unphysical (or second) Riemann sheet of the energy E. The pole wave functions of the second sheet are not square-integrable functions and they belong to decaying (capturing) resonances lying on the lower (upper) part of that energy sheet or antibound states lying on the negative real energy axis. The calculation of integrals in which these radial wave functions appear might need the use of a regularization procedure.

Since the number of basis states has to be finite the complex continuum has to be discretized. It is preferable to use as discretization points $E_i^{(p)}$ the abscissas of a Gaussian quadrature procedure. The corresponding weights of that procedure are denoted by h_i. By discretizing the integral in Eq. (7) one obtains an approximate completeness relation for the finite number of basis states:

$$\delta(r - r') \approx \sum_{n=b,d,c}^{M} w_n^{(p)}\big(r, E_n^{(p)}\big) w_n^{(p)}\big(r', E_n^{(p)}\big), \tag{8}$$

where c labels the discretized contour L^+ states. If $E_n^{(p)}$ corresponds to scattering energy from the contour L^+ then the scattering state of the discretized continuum is denoted by $w_n^{(p)}(r, E_n^{(p)}) = \sqrt{h_n} u_n^{(p)}(r, E_n^{(p)})$ and if $E_n^{(p)}$ corresponds to a normalized pole state then $w_n^{(p)}(r, E_n^{(p)}) = u_n^{(p)}(r)$. The set of Berggren vectors form a biorthonormal basis in the truncated space,

$$\big\langle \tilde{w}_n^{(p)} \big| w_m^{(p)} \big\rangle = \delta_{n,m}. \tag{9}$$

The Berggren basis for neutrons is defined similarly but the auxiliary problem uses the diagonal part of the second of Eqs. (4),

$$\big[K_l + V_0 + \tfrac{1}{2}(T_A - 1)V_1 - E_n^{(n)}\big] u_n^{(n)}(r) = 0. \tag{10}$$

Having fixed the Berggren basis for neutrons and protons we take the ansatz [Eq. (2)] and the relative motion functions are expanded on the corresponding Berggren bases

$$\phi_p(\mathbf{r}) = \left[\sum_{i=1}^{M_p} C_i^{(p)} w_i^{(p)}\big(r, E_i^{(p)}\big)\right] \mathcal{Y}_{ljm} \tag{11}$$

and

$$\phi_n(\mathbf{r}) = \left[\sum_{i=1}^{M_n} C_i^{(n)} w_i^{(n)}\big(r, E_i^{(n)}\big)\right] \mathcal{Y}_{ljm}, \tag{12}$$

where $\mathcal{Y}_{ljm}$ denotes the spin-angular part of the wave function. Using Eq. (4) we get the following set of linear equations for the unknown complex expansion coefficients $C_i^{(p)}$ and $C_i^{(n)}$:

$$\begin{aligned} &\big(E_k^{(p)} - \mathcal{E}_p\big) C_k^{(p)} + \sum_{m=1}^{M_n} \big\langle \tilde{w}_k^{(p)} \big| \delta v \big| w_m^{(n)} \big\rangle C_m^{(n)} = 0, \\ &k = 1, \ldots, M_p, \end{aligned} \tag{13}$$

and

$$\left[E_k^{(n)} - (\mathcal{E}_p - \Delta_c)\right] C_k^{(n)} + \sum_{m=1}^{M_p} \langle \tilde{w}_k^{(n)} | \delta v | w_m^{(p)} \rangle C_m^{(p)} = 0, \quad k = 1, \ldots, M_n, \tag{14}$$

where the coupling potential is $\delta v = \sqrt{\frac{T_A}{2}} V_1$. These two equations can be combined into one matrix eigenvalue equation with dimension $M_p + M_n$. By diagonalizing the matrix of the Hamiltonian we get $M_p + M_n$ complex eigenvalues, $\mathcal{E}_p^\nu$ $\nu = 1, \ldots M_p + M_n$. One of the complex eigenvalues $\mathcal{E}_p^\nu$ is identified by the energy of the IAR. The identification in general is easy to make because most of the other unbound states correspond to discretized contour states, they lie far from the position of the IAR at $\mathcal{E}_{\rm IAR} = E_r - i\frac{\Gamma}{2}$, and in the wave function of the IAR the dominant component is a bound neutron state.

C. Complex scaled Lane equations

The poles of the Green operator on the complex energy plane can be determined with the help of the complex scaling. The CS approach is mathematically well founded [18–20] and has many applications in atomic, molecular, and nuclear physics. We demonstrate the effect of CS on an example of a single-particle Hamiltonian $\hat{h}$. The real angle θ of the CS rotates the coordinates of the particle to the complex plane [i.e., $\mathbf{r}$ is simply replaced by $\exp(i\theta)\mathbf{r}$]. More precisely, the effect of CS can be given with the help of an operator $\hat{U}(\theta)$, which acts on an arbitrary function $g(\mathbf{r})$ as

$$\hat{U}(\theta) g(\mathbf{r}) = \exp\left(i\tfrac{3}{2}\theta\right) g(\mathbf{r}e^{i\theta}). \tag{15}$$

The complex scaled Hamiltonian is

$$\hat{h}_\theta = \hat{U}_\theta \hat{h} \hat{U}_\theta^{-1}. \tag{16}$$

The complex scaling transforms the kinetic energy $\hat{K} = -\frac{\hbar^2}{2\mu}\Delta_{\mathbf{r}}$ to

$$\hat{U}_\theta \hat{K} \hat{U}_\theta^{-1} = \exp(-i2\theta)\left(-\frac{\hbar^2}{2\mu}\Delta_{\mathbf{r}}\right), \tag{17}$$

and a local potential $\hat{V}(\mathbf{r})$ is transformed to the form

$$\hat{V}^\theta(\mathbf{r}) = \hat{U}_\theta \hat{V}(\mathbf{r}) \hat{U}_\theta^{-1} = \hat{V}[\mathbf{r}\exp(i\theta)]. \tag{18}$$

If we assume that $\chi_\nu(\mathbf{r})$ is a bound or resonance eigenfunction of the Hamiltonian $\hat{h}$ and the corresponding eigenvalue is E_ν then the function $\chi_\nu^\theta(\mathbf{r}) = \exp(i\frac{3}{2}\theta)\chi_\nu(\mathbf{r}e^{i\theta})$ will be the eigenfunction of the complex scaled Hamiltonian $\hat{h}_\theta$ with the same eigenvalue E_ν. The advantage of CS is that the function $\chi_\nu^\theta(\mathbf{r})$ is square integrable even if the original state was a resonant wave function. The square integrability of $\chi_\nu^\theta(\mathbf{r})$ allows it to be well approximated with finite expansion by using only square-integrable basis functions.

The Lane equations can be considered as an eigenvalue problem of a two-by-two matrix Hamiltonian

$$\mathcal{H} = \begin{pmatrix} K + V_0 - \frac{T_A}{2} V_1 + V_C & \sqrt{\frac{T_A}{2}} V_1 \\ \sqrt{\frac{T_A}{2}} V_1 & K + V_0 + \frac{T_A - 1}{2} V_1 + \Delta_c \end{pmatrix}. \tag{19}$$

The Lane equations [Eqs. (4)] can be cast into the form

$$\mathcal{H} \begin{pmatrix} \phi_p(\mathbf{r}) \\ \phi_n(\mathbf{r}) \end{pmatrix} = \mathcal{E}_p \begin{pmatrix} \phi_p(\mathbf{r}) \\ \phi_n(\mathbf{r}) \end{pmatrix}. \tag{20}$$

The generalization of the operator $\hat{U}_\theta$ is straightforward:

$$\mathcal{U}_\theta = \begin{pmatrix} U_\theta & 0 \\ 0 & U_\theta \end{pmatrix} \tag{21}$$

and the complex scaled matrix Hamiltonian is $\mathcal{H}_\theta = \hat{\mathcal{U}}_\theta \mathcal{H} \hat{\mathcal{U}}_\theta^{-1}$. The eigenvalue problem of this operator,

$$\mathcal{H}_\theta \begin{pmatrix} \phi_p^\theta(\mathbf{r}) \\ \phi_n^\theta(\mathbf{r}) \end{pmatrix} = \mathcal{E}_p^\theta \begin{pmatrix} \phi_p^\theta(\mathbf{r}) \\ \phi_n^\theta(\mathbf{r}) \end{pmatrix}, \tag{22}$$

in components gives the following set of equations:

$$\begin{aligned} \left[H_p^\theta - \mathcal{E}_p^\theta\right] \phi_p^\theta + \sqrt{\frac{1}{2} T_A} V_1^\theta \phi_n^\theta = 0, \\ \left[H_n^\theta - \mathcal{E}_p^\theta\right] \phi_n^\theta + \sqrt{\frac{1}{2} T_A} V_1^\theta \phi_p^\theta = 0, \end{aligned} \tag{23}$$

where $H_p^\theta = \exp(-i2\theta)K + V_0^\theta - \frac{1}{2}T_A V_1^\theta + V_C^\theta$ and $H_n^\theta = \exp(-i2\theta)K + V_0^\theta + \frac{1}{2}(T_A - 1)V_1^\theta + \Delta_c$. We will refer to Eqs. (23) as the complex scaled Lane equations. Since the functions $\phi_p^\theta(\mathbf{r})$ and $\phi_n^\theta(\mathbf{r})$ are square integrable we can make the approximations

$$\phi_p^\theta(\mathbf{r}) = \left[\sum_{i=1}^{M_p} C_i^{(p,\theta)} \psi_i^{(p)}(r)\right] \mathcal{Y}_{ljm} \tag{24}$$

and

$$\phi_n^\theta(\mathbf{r}) = \left[\sum_{i=1}^{M_n} C_i^{(n,\theta)} \psi_i^{(n)}(r)\right] \mathcal{Y}_{ljm}, \tag{25}$$

where $\psi_i^{(n)}(r)$ and $\psi_i^{(p)}(r)$ are arbitrary square-integrable basis functions. Substituting these forms into Eqs. (23) we get a matrix eigenvalue equation. In detail we have

$$\sum_{m=1}^{M_p} \langle \tilde{\psi}_k^{(p)} | H_p^\theta | \psi_m^{(p)} \rangle C_m^{(p,\theta)} + \sum_{m=1}^{M_n} \langle \tilde{\psi}_k^{(p)} | \delta v^\theta | \psi_m^{(n)} \rangle C_m^{(n,\theta)} = \mathcal{E}_p \sum_{m=1}^{M_p} \langle \tilde{\psi}_k^{(p)} | \psi_m^{(p)} \rangle C_m^{(p,\theta)}, \quad k = 1, \ldots, M_p, \tag{26}$$

and

$$\sum_{m=1}^{M_n} \langle \tilde{\psi}_k^{(n)} | H_n^\theta | \psi_m^{(n)} \rangle C_m^{(n,\theta)} + \sum_{m=1}^{M_p} \langle \tilde{\psi}_k^{(n)} | \delta v^\theta | \psi_m^{(p)} \rangle C_m^{(p,\theta)} = \mathcal{E}_p \sum_{m=1}^{M_n} \langle \tilde{\psi}_k^{(n)} | \psi_m^{(n)} \rangle C_m^{(n,\theta)}, \quad k = 1, \ldots, M_n. \tag{27}$$

TABLE I. Energies of the discrete $g_{9/2}$ single-particle basis states for neutrons and for protons corresponding to the Woods-Saxon potential described in the text. The Coulomb potential for protons is either the usual one in Eq. (30) or the dilation analytic one in Eq. (32). Energies are in MeV.

State	Neutron	Proton [Eq. (30)]	Proton [Eq. (32)]
$1g_{9/2}$	$(-22.878, 0.0000)$	$(-11.894, 0.0000)$	$(-13.975, 0.0000)$
$2g_{9/2}$	$(-4.060, 0.0000)$	$(7.674, -6.2 \times 10^{-4})$	$(6.070, -2.0 \times 10^{-5})$

The solution of these equations provides us with $M_p + M_n$ complex eigenvalues. The majority of these eigenvalues correspond to the discretization of the rotated continua. The bound and resonance poles can be clearly identified and the accurate value can be determined by using the so-called θ trajectory technique.

III. NUMERICAL RESULTS

We applied the methods described in Sec. II B and II C for the description of the IARs in the ^{209}Bi nucleus with large neutron excess. We studied several analog resonances in the $p + {}^{208}$Pb system. For illustrative purposes we selected an IAR that in our simple model is the analog of the ground state of ^{209}Pb (i.e., a $g_{9/2}$ single-particle state). The effect of the double magic core is described by a phenomenological potential. We used Woods-Saxon (WS) forms for both the diagonal and the coupling potentials in Eqs. (4). The WS forms cut to zero at a finite distance ($R_{\max} = 20$ fm):

$$V_{\rm tr}^{\rm WS}(r) = \begin{cases} V^{\rm WS}(r) & \text{if} \quad r < R_{\max}, \\ 0 & \text{if} \quad r \geqslant R_{\max}. \end{cases} \tag{28}$$

The spin-orbit part of the potential has the usual derivative form

$$V_{\rm so}^{\rm WS}(r) = -\frac{V_{\rm so}}{ra} 2(\vec{l}\cdot\vec{s}) \frac{e^{\frac{r-R}{a}}}{(1+e^{\frac{r-R}{a}})^2}. \tag{29}$$

It is also cut to zero at $R_{\max}$. The numerical values of the potential parameters were taken from an early work [35]. For the sake of simplicity, the same values for the radii and the diffuseness and for the common spin-orbit term for protons and neutrons were taken: $r_0 = 1.19$ fm, $a = 0.75$ fm, and $V_{\rm so} = 11.6$ MeV. For Coulomb potential we assumed that the charge Ze of the target is homogeneously distributed inside a sphere with radius $R_c = r_c A^{1/3}$ with sharp edge

$$V_C(r) = Ze^2 \begin{cases} \frac{1}{2R_c}\left[3 - \left(\frac{r}{R_c}\right)^2\right] & \text{if} \quad r \leqslant R_c, \\ 1/r & \text{if} \quad r > R_c. \end{cases} \tag{30}$$

The depth of the nucleon potential was 56.4 MeV and the strength of the symmetry potential was 0.5 MeV. Therefore the diagonal WS potential felt by the proton was 61.9 MeV and by the neutron 51.15 MeV, according to the Lane equations [Eqs. (4)]. The Coulomb radius was identical with the one for the nuclear potential. The Coulomb energy difference was also the same as in Ref. [35] ($\Delta_c = 18.9$ MeV).

In the CXSM method the elements of the single-particle bases are calculated in the diagonal potentials appearing in the corresponding channels of the Lane equations. The single-particle energies for the $g_{9/2}$ neutron and proton orbits are summarized in Table I. The vertexes of three different proton and neutron L contours for the $g_{9/2}$ case are shown in Table II. The numbers of the discretization points N_i of the segment $[V_i, V_{i+1}]$ are shown between the vertex points. To calculate IARs we could use neutron contours taken along the

TABLE II. Integration contours for $g_{9/2}$ protons and neutrons given by vertexes V_i (in MeV) and the number of Gaussian points N_i. The N_i values are the ones necessary to reach the 1-keV accuracy for the IAR or for the broad resonance at $\mathcal{E}_p = (23.996, -6.147)$ MeV. Contours LP3 and LN3 were used for the broad resonance.

Channel contour	Proton			Neutron		
	LP1	LP2	LP3	LN1	LN2	LN3
V_0	(0, 0)	(0, 0)	(0, 0)	(5, −0.4)	(5, −0.35)	(3, 0)
N_0	0	0	4	0	0	10
V_1	(5, −0.4)	(5, −0.35)	(5, −0.4)	(30, −0.4)	(30, −2.098)	(3, −10)
N_1	78	34	22	0	0	4
V_2	(30, −0.4)	(30, −2.098)	(30, 0)	(30, 0)	(100, −6.993)	(10, −10)
N_2	2	4	2	0	0	6
V_3	(30, 0)	(100, −6.993)	(100, 0)	(100, 0)		(10, 0)
N_3	0		4	0	0	4
V_4	(100, 0)		(200, 0)	(200, 0)		(30, 0)
N_4	0			0	0	0
V_5	(200, 0)					(100, 0)

TABLE III. Comparison of the IAR parameters calculated by using the CC and CXSM methods for different partial waves with Coulomb potential Eq. (30). Energies are in MeV units.

lj	E_r (CXSM)	E_r (CC)	Γ (CXSM)	Γ (CC)
$g_{9/2}$	14.954	14.954	0.046	0.047
$i_{11/2}$	15.526	15.526	0.003	0.003
$d_{5/2}$	16.445	16.444	0.141	0.140
$s_{1/2}$	16.918	16.917	0.156	0.156
$g_{7/2}$	17.367	17.367	0.086	0.084
$d_{3/2}$	17.441	17.440	0.144	0.145
$j_{15/2}$	18.774	18.774	0.006	0.006

real axis. For other partial waves we used a large variety of contours.

In the CC method we solved the coupled Lane equations for a fine equidistant mesh of the bombarding proton energy $\mathcal{E}_p = \mathcal{E}_0, \mathcal{E}_0 + d\mathcal{E}, \ldots, \mathcal{E}_{\max}$ in the center-of-mass system and calculated the scattering matrix elements, $S(\mathcal{E}_p)$, for each energy value.

To determine the parameters of the IAR we fitted the tabulated values of the $S(\mathcal{E}_i)$ by the following form:

$$S(\mathcal{E}_p) = e^{2i\delta_p(\mathcal{E}_p)}\left(1 - i\frac{\Gamma_p}{\mathcal{E}_p - \mathcal{E}_{\mathrm{IAR}}}\right), \tag{31}$$

where $\mathcal{E}_{\mathrm{IAR}}$ denotes the complex energy of the IAR (i.e. $\mathcal{E}_{\mathrm{IAR}} = E_r - i\frac{\Gamma}{2}$), Γ is the full width, and Γ_p is the proton partial width of the IAR. Below the threshold of the ^{208}Pb$(p,\bar{n})^{208}$Bi reaction the total width is equal to the the partial width: $\Gamma = \Gamma_p$ in our model. Equation (31) represents a one-pole approximation to the S matrix in the proton channel.

For the background phase shift in the entrance channel $\delta_p(\mathcal{E}_p)$ we take a linear energy dependence to better reproduce the nonresonant background. Naturally all these quantities refer to definite l, j partial waves. The best-fit parameter values are listed in the E_r (CC) and Γ (CC) columns in Table III. The one-pole formula of Eq. (31) gave an excellent fit to the tabulated values of $S(\mathcal{E}_i)$ in all cases in Table III.

The numerical values of $\mathcal{E}_{\mathrm{IAR}}$ are shown as E_r (CXSM) and Γ (CXSM) in Table III in comparison with the results extracted from the solution of the coupled Lane equations, E_r (CC) and Γ (CC). As one can see from the comparison the positions and the widths calculated by the CXSM agree well (within 1 keV) with the result of the CC method.

Let us discuss briefly how this agreement has been achieved. We optimized the shape of the contours and the number of points along the contours separately for neutrons and protons and for different partial waves. The shape of the contour is fixed by the vertexes, which were chosen to be able to include the narrowest single-particle resonant states. We observed that the contour should not get close either to the energies of the resonances included in the basis or to the IAR result from the diagonalization. The last vertex point (i.e., the energy of the last segment with $N_i \neq 0$) was crucial to get good agreement for both the real and the imaginary parts of the IAR energy calculated by solving the Lane equations.

We tested the convergence of the IAR energies by increasing the number of discretization points and stopped to increase it when the energy did not change. After that, we continued with the next interval and increased the points of that interval similarly. After going through all the intervals we optimized the number of mesh points by reducing them until the energy in keV did not change. We also tested the convergence of the IAR energies by varying the positions of the vertexes. If the contour goes very far from the real axis (i.e., if we choose the value of the imaginary parts of the vertexes considerably larger than the ones in Table II) then the degree of agreement might be spoiled even if we choose more discretization points. We found for all partial waves that the IARs are not very sensitive to the low-energy part of the continuum (below 5 MeV), neither for neutrons nor for protons. At high energy however a cutoff smaller than 30 MeV affects the convergence of the IAR energy.

To be able to compare pole solutions for calculation of the resonance parameters of the IAR we repeated the calculation by applying CS for the solution of the Lane equations. Unfortunately, the Coulomb potential of a charged sphere with sharp edge is not dilation analytic because this form becomes discontinuous for $\theta \neq 0$. We used the Coulomb potential expressed by the error function, which is dilation analytic. For the Coulomb potential the form

$$V_C(r) = Ze^2\frac{\mathrm{Erf}(r/\alpha)}{r} \tag{32}$$

is widely used in both atomic and nuclear physics [26,36]. In the resonating group model it can be obtained as the direct folding interaction between nuclei [37]. The numerical value of the parameter $\alpha = 0.31$ fm was adjusted to the Coulomb potential in Eq. (30). For the nuclear potential we kept the WS form, which is dilation analytic until the rotation angle is below the critical angle [$\theta < \theta_{\mathrm{crit}} = \arctan(\frac{a\pi}{R})$].

For the solution of the complex scaled Lane equations we used the Laguerre mesh basis functions

$$\psi_i^{(\nu)}(r) = (-1)^i r_i^{-1/2}\frac{rL_{M_\nu}(r)}{r - r_i}\exp(-r/2), \tag{33}$$

where $\nu = p, n$. The mesh points are given by $L_{M_\nu}(r_i) = 0$, where $L_{M_\nu}(r)$ is the Laguerre polynomial. The advantage of this basis is that the matrix elements of any local potential is extremely simple [38]. This type of basis function has proved to be very accurate both in simple model calculations and in three-body problems [38–40]. One can introduce an additional simple scaling parameter of the basis [38] for this parameter; we used the 0.3 fm value.

The agreement between the pole positions calculated by the CXSM and the CS methods is extremely good for all partial waves, as shown in Table IV. One can see that the agreement with the numerically exact solution of the Lane equations (CC) is as good as in the previous case when the CXSM was used with the standard Coulomb potential. The maximal difference does not exceeds 1 keV.

To understand better the formation of the IAR let us consider again the $l = 4$, $j = 9/2$ case as an example. In Fig. 2 we show the positions of the unperturbed states forming the Berggren basis (denoted by circles for neutrons and squares for protons) and some of the results of the diagonalization (with perturbed states denoted by filled circles) on the complex

TABLE IV. Comparison of the IAR parameters calculated by using the CC, CXSM, and CS methods for different partial waves with the dilation analytic Coulomb potential Eq. (32). Energies are in MeV units.

lj	E_r (CXSM)	E_r (CS)	E_r (CC)	Γ (CXSM)	Γ (CS)	Γ (CC)
$g_{9/2}$	14.933	14.933	14.934	0.041	0.041	0.042
$i_{11/2}$	15.493	15.493	15.493	0.002	0.002	0.002
$d_{5/2}$	16.436	16.436	16.444	0.121	0.120	0.120
$s_{1/2}$	16.913	16.913	16.913	0.127	0.127	0.128
$g_{7/2}$	17.350	17.349	17.349	0.076	0.075	0.074
$d_{3/2}$	17.434	17.434	17.433	0.118	0.119	0.120
$j_{15/2}$	18.752	18.751	18.752	0.005	0.005	0.005

energy plane. A section of the real E-axis and of the lower half of the complex plane is shown. In this case the neutron contour is along the real axis and the proton contour has a trapezoidal shape with vertexes denoted by LP1 in Table II. To better highlight the region of our interest the states with energies higher than 60 MeV are not shown in Fig. 2. The discrete basis states are listed in Table I. The bound basis states are the $1g_{9/2}$ proton state at $E_i^{(p)} = -13.975$ MeV and the two neutron states $1g_{9/2}$, $2g_{9/2}$ at $E_i^{(n)} = -22.878$ MeV and at $E_i^{(n)} = -4.060$ MeV, which are shifted upward by $\Delta_c = 18.9$ MeV. The narrow $2g_{9/2}$ proton resonance at $E_i^{(p)} = (6.070, -2 \times 10^{-5})$ MeV seems to lie on the real axis.

Most of the perturbed states lie close to the positions of the corresponding basis states since the coupling symmetry potential term causes only a small shift for these states. One exception is the IAR at $\mathcal{E}_{\rm IAR} = (14.933, -0.021)$ MeV, which shifted downward well below the bound $2g_{9/2}$ neutron state, which is the main component of its wave function $C_i^{(n)} = (0.9921, -0.0047)$. The second largest component is that of the $2g_{9/2}$ proton resonance with $C_i^{(p)} = (-0.1194, 0.0002)$. The other perturbed states that do not fit to the path of the contours are states based on contour states but fall off the contour because of the finite number of discretization points.

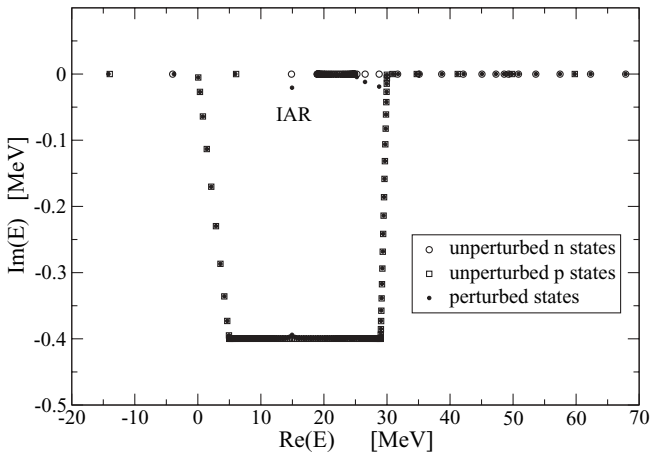

FIG. 2. Positions of the $g_{9/2}$ Berggren basis states (circles for neutrons and squares for protons) and the results of the CXSM method (filled circles) on the complex E-plane for the Coulomb potential Eq. (30).

If the number of discretization points is increased they move closer to the contour. They also move with the contour if we change the shape of the contour, in contrast to the IAR, which remains in the same position. Of course the IAR should lie above the proton contour to be explored. This feature is very similar to the one observed in the CS calculation.

From the mathematical theory of the complex scaling [18–22] it is known that the continuous part of the spectrum of the complex scaled Hamilton operator consists of half lines on the complex energy plane. The half lines start at the thresholds and they are rotated downward from the real axis by 2θ. In our calculation we have used $M_p = M_n = 100$ basis functions and received 200 approximate complex eigenvalues from the diagonalization. These eigenvalues are plotted on Fig. 3 for two different θ values ($\theta = 2^\circ$ and $\theta = 4^\circ$). From this figure it is obvious that the vast majority of the eigenvalues correspond to discretization of the continuous spectrum. However, there are a few eigenvalues that are independent of the complex scaling parameter θ. These are denoted by letters b_1, b_2 and r_1, r_2 in Figure 3(a). Here r_2 is the IAR, which is based mainly on the $2g_{9/2}$ bound neutron state as we have seen in the CXSM calculation before. The r_1 resonance is based mainly on the narrow $2g_{9/2}$ proton resonance at $E_i^{(p)} = (6.070, -2 \times 10^{-5})$ MeV. The bound states b_1 and b_2 originate on the $1g_{9/2}$ proton state at $E_i^{(p)} = -13.975$ MeV and the $1g_{9/2}$ neutron state at $E_i^{(n)} = -22.878$ MeV, which are shifted upward by $\Delta_c = 18.9$ MeV.

Figure 3(b) shows the so-called θ trajectory (i.e., the complex energy plane in the vicinity of the IAR when the complex scaling parameter changes between $\theta = 2^\circ$ and $\theta = 8^\circ$ with step size of 1°). There is a small change in the position and width of the resonance (which should be independent of the value of θ) but this comes from the fact that a finite basis is used. This phenomena is well known in all complex scaling calculations and there are methods on how to select the best approximation for the resonance [41]. The resonance position and width values given in Table IV correspond to calculations with $\theta = 4^\circ$.

The CXSM and the CS methods are similar in that results become less accurate if the contour of the CXSM or the rotated half lines lie close to the resonance. To get high accuracy the resonance has to be well explored (i.e., should lie far above the contour). The rotated half lines of the CS play a role similar to that of the contours of the CXSM;

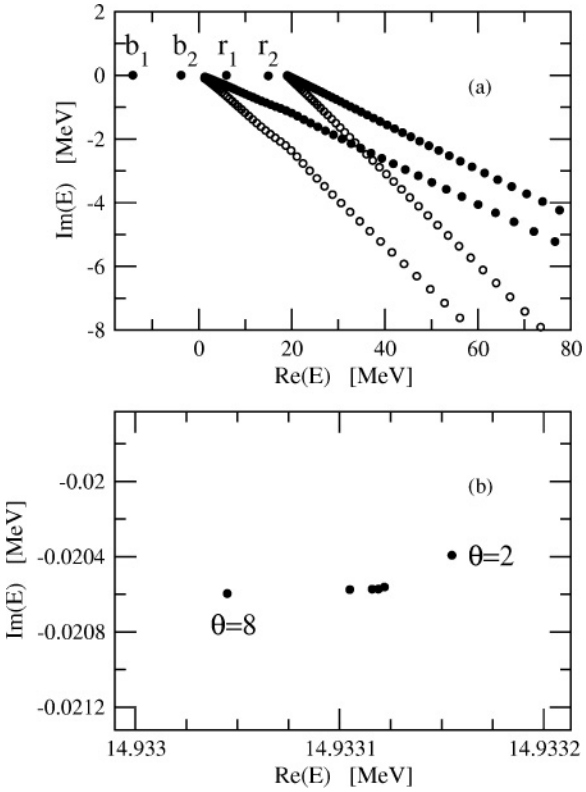

FIG. 3. (a) Positions of the $g_{9/2}$ states on the complex E-plane with the CS method with a rotation angle of $\theta = 2^\circ$ (filed circles) and with $\theta = 4^\circ$ (open circles) for the Coulomb potential Eq. (32). The IAR is the state r_2. (b) The vicinity of the IAR, in which the CS scaling parameter θ is varied between 2° and 8° with a step size of 1°.

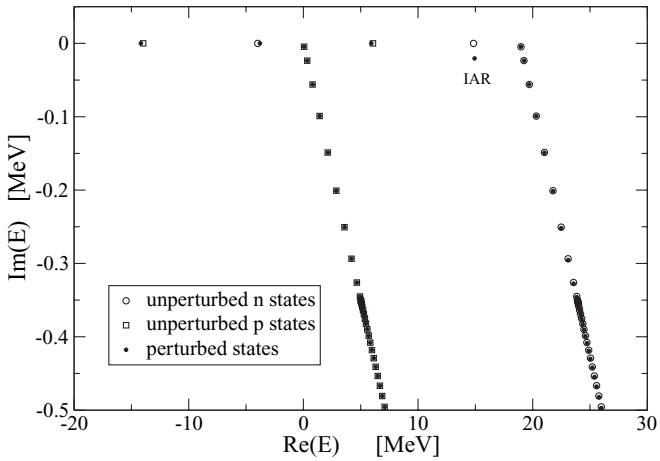

FIG. 4. Positions of the $g_{9/2}$ Berggren basis states (circles for neutrons and squares for protons) and the results of the CXSM method (filled circles) on the complex E-plane for the Coulomb potential Eq. (32) with contours LP2 and LN2 in Table II. They are similar to the optimal contour of the CS method.

therefore we shall call the half lines of the CS method contours as well. Only the resonances above the contours can be calculated. This means that the $3g_{9/2}$ neutron resonance at $E^{(n)} = (4.929, -6.035)$ $\arg(E^{(n)}) = 50.76^\circ$ or the corresponding perturbed solution cannot be calculated by the CS method since they cannot be explored because of the critical angle of the WS potential, $\theta_{\rm crit} = 18.48^\circ$. It can be calculated however by the CXSM method by using contours LP3 − LN3; we get for the perturbed energy $\mathcal{E}_p = (23.996, -6.147)$ MeV $\arg(\mathcal{E}_p - \Delta_c) = 50.33^\circ$.

The similarity of the methods can be seen even better if we try to use a contour in the CXSM that resembles the rotated continuum of the CS calculation. In Fig. 4 we present the results of the CXSM calculation in which the contours LP2 and LN2 were chosen to be the same as the one corresponding to the optimal $\theta = 4^\circ$ rotational angle of the CS calculation. One can see that the IAR is well separated from the two contours starting at the origin and the one starting at the neutron emission threshold. The unperturbed pole closest to the IAR is the bound $2g_{9/2}$ neutron state, which is the dominating component of the IAR wave function with amplitude $C_i^{(n)} = (0.9918, -0.0043)$. The second largest component of the IAR wave function is that of the $2g_{9/2}$ proton resonance with amplitude $C_i^{(p)} = (-0.1194, 0.0001)$. The wave function of the IAR is practically unchanged as far as the discrete components are concerned with respect to the case with the contours used in Fig. 2 (LP1 and a real neutron contour). The energy of the IAR is $\mathcal{E}_p = (14.93309, -0.02058)$ MeV, which coincides with the value of $\mathcal{E}_p = (14.93303, -0.02062)$ MeV with the contours used in Fig. 2 within the numerical error of 1 keV estimated from the deviation from the CC results in Table IV. This good agreement convinces us that the use of the LP2 and LN2 contours, which resemble the contour of the CS, could also be used for calculating the IAR. The components of the different scattering states taken from the different contours are certainly very different but the summed contribution of the proton and neutron contours is basically the same. Since both are small numbers their numerical values have little importance. For the $g_{9/2}$ IAR the neutron continuum has negligible effect. For other partial waves this effect is also small but not completely negligible.

An important difference between the results presented in Figs. 3 and 4 is that in Fig. 3 only perturbed states are shown since in the CS method the basis states used are not eigenstates of any unperturbed Hamiltonians. Therefore from the coefficients of the wave function of the IAR explored we cannot estimate the role of the unperturbed neutron and proton states easily. To get similar quantities we have to calculate the unperturbed state with the same CS contour and we have to calculate overlaps with the IAR wave function.

IV. SUMMARY

Let us summarize briefly the results we obtained in this study. We reproduced the results of the direct numerical solution of the coupled Lane equations by diagonalizing the Hamiltonian in the full n-p Berggren basis (i.e., by using the CXSM method). The IAR parameters were extracted from the $S(\mathcal{E}_p)$ calculated by solving the Lane equations along the real $\mathcal{E}_p$-axis by fitting it using the one-pole approximation [Eq. (31)]. The fitted position E_r (CC) and the width Γ (CC) of the IAR were compared to the results of the CXSM calculation

and the agreement was generally better than 1 keV for all partial waves in which we had IARs. In the wave function of the IAR furnished by the CXSM the contribution of the bound neutron state has the dominant role and the proton resonance has a non-negligible effect. The integrated effect of the proton continuum is small but essential to produce the correct width for the resonance. We studied the details of the different parts of the continuum segments and the necessary numbers of the discretization points on the different segments. The roles of the cutoff energy and the low-energy part of the continuum were also investigated. The neutron continuum had a very small effect for the IARs.

The pole position of the IAR was calculated by the complex scaling method as well. For that we modified the Coulomb potential for a dilational analytic one and repeated the CC calculation and CXSM method with the modified Coulomb potential. We obtained very good agreement to the numerical solution of the coupled Lane equations with both the CXSM and the CS methods. Therefore we conclude that in this case the CXSM and the CS methods give basically the same results, apart from some numerical errors, which naturally were not the same in the two types of calculations. This agreement suggests that the two methods are basically equivalent in those cases when both methods can be applied.

Besides the similarities and differences of the CXSM and the CS methods discussed so far there are important differences between them. The application of the uniform CS method used here is restricted to dilation analytic potentials and the range of the rotational angle could also be limited. However, in the CXSM method the shape of the contour can be chosen with great flexibility, although to go too deep into the complex energy might somewhat spoil the accuracy of the calculated results. Another advantage of the CXSM is that the structure of the resonant state can be seen directly from the coefficients of the perturbed wave function. In the CS method the same information can be explored in a more indirect way.

To be able to compare the result of our powerful CXSM method to measured cross sections we have to extend our method for complex potentials, which could account for the flux of the particles into reaction channels not explicitly included in the Lane model. Therefore we plan to use complex potentials in the CXSM and calculate partial and spreading widths of the resonances. For taking realistic values for the isoscalar and isovector parts of the nucleon-nucleus optical potential, classical works in Refs. [42,43] and the results of the recent systematics in Ref. [44] might be useful.

ACKNOWLEDGMENTS

Discussions with R. G. Lovas and R. J. Liotta are gratefully acknowledged. This work has been supported by PICT 21605 (ANPCyT-Argentina), by the Hungarian OTKA funds Nos. K72357 and T46791, and by the Hungarian-Argentinian governmental fund No. NKTH Arg-6/2005-SECYT HU/PA05-EIII/005.

[1] T. Teranishi *et al*., Phys. Lett. **B407**, 110 (1997).
[2] S. Takeuchi *et al*., Phys. Lett. **B515**, 255 (2001).
[3] G. V. Rogachev *et al*., Phys. Rev. C **67**, 041603(R) (2003).
[4] G. V. Rogachev *et al*., Phys. Rev. Lett. **92**, 232502 (2004).
[5] R. Id Betan, R. J. Liotta, N. Sandulescu, and T. Vertse, Phys. Rev. Lett. **89**, 042501 (2002).
[6] R. Id Betan, R. J. Liotta, N. Sandulescu, and T. Vertse, Phys. Rev. C **67**, 014322 (2003).
[7] N. Michel, W. Nazarewicz, M. Ploszajczak, and K. Bennaceur, Phys. Rev. Lett. **89**, 042502 (2002).
[8] N. Michel, W. Nazarewicz, M. Ploszajczak, and J. Okolowicz, Phys. Rev. C **67**, 054311 (2003).
[9] N. Michel, W. Nazarewicz, and M. Płoszajczak, Phys. Rev. C **75**, 031301(R) (2007).
[10] N. Michel, W. Nazarewicz, and M. Płoszajczak, Nucl. Phys. **A794**, 29 (2007).
[11] J. Rotureau, N. Michel, W. Nazarewicz, M. Płoszajczak, and J. Dukelsky, Phys. Rev. Lett. **97**, 110603 (2006).
[12] T. Berggren, Nucl. Phys. **A109**, 265 (1968).
[13] R. Id Betan, N. Sandulescu, and T. Vertse, Nucl. Phys. **A771**, 93 (2006).
[14] G. G. Dussel, R. Id Betan, R. J. Liotta, and T. Vertse, Nucl. Phys. **A789**, 182 (2007).
[15] T. Vertse, R. J. Liotta, and E. Maglione, Nucl. Phys. **A584**, 13 (1995).
[16] J. Blomqvist, O. Civitarese, E. D. Kirchuk, R. J. Liotta, and T. Vertse, Phys. Rev. C **53**, 2001 (1996).
[17] R. J. Liotta, E. Maglione, N. Sandulescu, and T. Vertse, Phys. Lett. **B367**, 1 (1996).
[18] J. Aguilar and J. M. Combes, Commun. Math. Phys. **22**, 269 (1971).
[19] E. Balslev and J. M. Combes, Commun. Math. Phys. **22**, 280 (1971).
[20] B. Simon, Commun. Math. Phys. **27**, 1 (1971).
[21] Y. K. Ho, Phys. Rep. **99**, 1 (1983).
[22] N. Moiseyev, Phys. Rep. **302**, 211 (1998).
[23] A. M. Lane, Nucl. Phys. **A35**, 676 (1962).
[24] G. Colo, H. Sagawa, N. Van Giai, P. F. Bortignon, and T. Suzuki, Phys. Rev. C **57**, 3049 (1998).
[25] R. F. Barett, B. A. Robson, and W. Tobocman, Rev. Mod. Phys. **55**, 155 (1983).
[26] T. Myo, A. Ohnishi, and K. Katō, Prog. Theor. Phys. **99**, 801 (1998).
[27] G. Hagen and J. S. Vaagen, Phys. Rev. C **73**, 034321 (2006).
[28] N. Michel, W. Nazarewicz, and M. Płoszajczak, Phys. Rev. C **70**, 064313 (2004).
[29] N. Michel, J. Math. Phys. **49**, 022109 (2008).
[30] R. Id Betan, R. J. Liotta, N. Sandulescu, T. Vertse, and R. Wyss, Phys. Rev. C **72**, 054322 (2005).
[31] N. Michel, W. Nazarewicz, M. Płoszajczak, and J. Rotureau, Phys. Rev. C **74**, 054305 (2006).
[32] Ya. B. Zel'dovich, ZhETF (USSR) **39**, 776 (1960).
[33] W. J. Romo, Nucl. Phys. **A116**, 617 (1968).
[34] B. Gyarmati and T. Vertse, Nucl. Phys. **A160**, 523 (1971).
[35] B. Gyarmati and T. Vertse, Nucl. Phys. **A182**, 315 (1972).
[36] J. Toulouse, Phys. Rev. B **72**, 035117 (2005).

[37] S. Saito, Suppl. Prog. Theor. Phys. **62**, 11 (1977).
[38] D. Baye, M. Hesse, and M. Vincke, Phys. Rev. E **65**, 026701 (2002).
[39] D. Baye and P.-H. Heenen, J. Phys. A **19**, 2041 (1986).
[40] D. Baye, Nucl. Phys. **A627**, 305 (1997).
[41] R. Yaris and P. Winkler, J. Phys. B **11**, 1475 (1978).
[42] F. A. Brieva and R. G. Lovas, Nucl. Phys. **A341**, 377 (1990).
[43] J. D. Carlson, D. A. Lind, and C. D. Zafiratos, Phys. Rev. Lett. **30**, 99 (1973).
[44] G. C. Jon, H. Orihara, C. C. Yun, A. Terakawa, K. Itoh, A. Yamamoto, H. Suzuki, H. Mizuno, G. Kamurai, K. Ishii, and H. Ohnuma, Phys. Rev. C **62**, 044609 (2000).